Guiding, Focusing, and Sensing on the Subwavelength Scale Using Metallic Wire Arrays

G. Shvets* and S. Trendafilov
Department of Physics, The University of Texas at Austin, Austin, Texas 78712, USA

J. B. Pendry
Blackett Laboratory, Imperial College, Prince Consort Road, London SW7 2BW, United Kingdom

A. Sarychev
Ethertronics Inc., San Diego, California 92121, USA

(Received 5 February 2007; revised manuscript received 16 May 2007; published 2 August 2007)

We show that tapered arrays of thin metallic wires can manipulate electromagnetic fields on the subwavelength spatial scale. Two types of nanoscale imaging applications using terahertz and midinfrared waves are enabled: image magnification and radiation focusing. First, the tapered wire array acts as a multipixel TEM endoscope by capturing an electromagnetic field profile created by deeply subwavelength objects at the endoscope's tip and magnifying it for observation. Second, the image of a large mask at the endoscope's base is projected onto a much smaller image at the tip.

DOI: 10.1103/PhysRevLett.99.053903 PACS numbers: 42.82.Et, 41.20.Jb, 42.79.Pw, 84.40.Az

Diffraction of light is the major obstacle to a variety of applications requiring concentrating optical energy in a small volume: light cannot be confined to dimensions much smaller than half of its wavelength $\lambda/2$. Applications that would benefit from overcoming the diffraction limit include nonlinear spectroscopy and harmonics generation [1–4], subwavelength optical waveguiding [5–7], and nanofabrication [8]. Utilizing plasmonic materials with negative dielectric permittivity circumvents the diffraction limit. Examples of diffraction-beating devices based on plasmonics include superlenses [9–12], coupled-sphere waveguides [13], sharp focusing tips [14], and resonantly excited arrays of metal wires [15].

High losses associated with surface plasmonics are hampering many of these applications. Another challenge yet to be met is designing practical imaging modalities based on sub-λ plasmons that convert near-field electromagnetic (EM) perturbations into the far field for easy observation. In this Letter we propose a solution to these two problems: a tapered multiwire array supporting subwavelength transverse electromagnetic (TEM) waves. Examples of the multiwire endoscopes based on such arrays (untapered and tapered) are shown in Fig. 1. We demonstrated that the tapered endoscope can accomplish two tasks: (i) creating near the *base* of an endoscope a magnified image of deeply subwavelength objects (metal spheres, in our case) placed at the endoscope's *tip*, and (ii) creating near the *tip* of an endoscope a reduced image of a mask placed at the endoscope's *base*. Accomplishing the first task is necessary for making a sub-λ sensor while accomplishing the second one – for making a sub-λ lithographic tool. Although the lack of the cutoff of the TEM transmission lines has been exploited in the past [16,17] for guiding on a subwavelength scale, this Letter demonstrates, for the first time, how the subwavelength image can be manipulated by tapering the coaxial endoscope. We also demonstrate that TEM modes of a multiwire perfectly electrically conducting (PEC) transmission line have a low-loss dispersionless plasmonic counterpart in the optical part of the spectrum paving the way to novel optical applications.

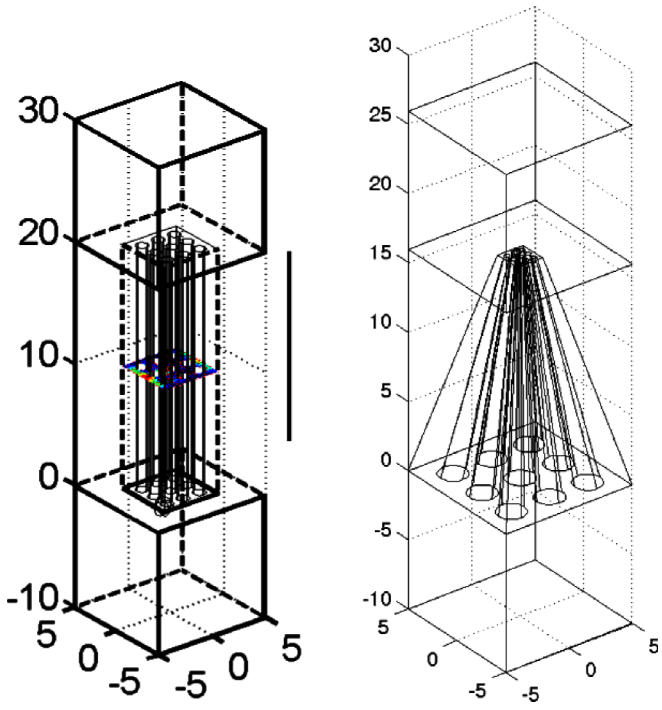

FIG. 1 (color online). Schematics of two subwavelength endoscopes based on a 3×3 array of metal wires embedded in a straight (left) or tapered (right) metal-coated fiber. Both endoscopes are terminated by square single-mode rectangular waveguides on both ends.

Single metallic wires and coaxial wire cones have recently attracted considerable attention as low-loss waveguides [18,19] of TEM-like modes of THz and far-infrared radiation. Using a single wire waveguide has its limitations: for example, if a wire is used as a high spatial resolution sensor, then only a single bit of information can be collected without scanning the wire. In contrast, an array of closely spaced wires can act as a multichannel sensor capable of simultaneously collecting information from a spatially distributed object. Electromagnetic properties of metallic wire arrays have been previously investigated in the context of metamaterials [20–23]. Below we review the electromagnetic properties of an infinite square array with period d of straight (along the z direction) PEC wires of an arbitrary shape in the x-y plane. Three types of waves with the propagation wave number k_z, transverse wave number $\vec{k}_\perp$, and frequency ω are supported by the array: transverse magnetic (TM), transverse electric (TE), and TEM modes. The transverse Bloch wave number $\vec{k}_\perp \equiv k_x\vec{e}_x + k_y\vec{e}_y$, where $\vec{F} \equiv \{\vec{E}, \vec{B}\}$ satisfies the phase-shifted boundary conditions (PSBC): $\vec{F}(x = d/2, y) = \exp(ik_x d)\vec{F}(x = -d/2, y)$ and $\vec{F}(x, y = d/2) = \exp(ik_y d)\vec{F}(x, y = -d/2)$. TM modes are always evanescent (i.e., k_z is imaginary) for sub-λ arrays with $\omega d/c < 1$ [20]. The dispersion relation for the TE modes is shown in Fig. 2 as the blue dashed line for the infinite array of PEC wires with the period $d = \lambda/10$ and diameter $w = \lambda/15$ imbedded in glass with the dielectric permittivity $\epsilon_d = 2.25$. Clearly, for large $|\vec{k}_\perp| > \omega/c$ corresponding to sub-λ feature sizes TE modes are also evanescent.

The remaining waves are the *always propagating* TEM modes of the periodic metal cylinder array with a very simple dispersion relation: $\epsilon_d\omega^2(k_z, \vec{k}_\perp) \equiv k_z^2c^2$. Electric and magnetic fields of the TEM wave are orthogonal to each other and given by $\vec{E} = \vec{\nabla}_\perp\phi$ and $\vec{B} = \vec{e}_z \times \vec{\nabla}_\perp\phi$, where $\phi(\vec{x}_\perp)_{\vec{k}_\perp}$ satisfies the PSBC and $\phi = \text{const}$ at the metal surface. The remarkable property of the TEM waves of being dispersionless with respect to the transverse wave number $\vec{k}_\perp$ can be explored in subwavelength guiding or imaging applications. Therefore, TEM modes are *transversely local*: the image of an object with finite transverse size does not spread out as it is transported along the endoscope. For a *finite* $N \times N$ array of wires surrounded by a perfectly conducting metal shell, there are N^2 distinct wave numbers supported by the array [16], regardless of the array size N. Therefore, TEM modes of an endoscope consisting an $N \times N$ wire bundle are capable of transferring N^2 "pixels" along its length.

An ideal endoscope transfers an arbitrary image of the field distribution at $z = 0$ over a significant distance to $z = L$ with minimal distortion. However, if the total cross section of the tapered endoscope becomes smaller than $\lambda^2/4$, then all TE and TM modes are evanescent. The only modes that can transport the image without distortion are the TEM modes. Because they do not form a complete set, they can only enable spatial resolution of order the wire spacing d. Therefore, imaging with TEM waves is a form of discrete sampling: the exact spatial profile of a small scatterer with a spatial dimension $\Delta \ll d$ will not be resolved in the image, but its presence in a specific $d \times d$ unit cell will be detected. Making the spacing d extremely subwavelength results in an arbitrary high spatial resolution.

To illustrate imaging properties of a multiwire endoscope, we have numerically simulated the following problem: transferring an image of a metallic sphere with a diameter $D = \lambda/10$ using a 3×3 array of conducting wires encased in a square $\lambda/3 \times \lambda/3$ subwavelength metal waveguide. Wire spacing and diameter are $d = \lambda/10$ and $w = \lambda/15$, endoscope's length is $L = 4\lambda/3$. All simulations in this Letter are made under a simplifying assumption of perfectly electrically conducting (PEC) metals. As shown at the end of the Letter, this assumption is valid for EM waves spanning mid-IR and THz frequency ranges. PEC boundary conditions make the results scalable to any wavelength. Therefore, all dimensions are scaled to an arbitrary length scale $L_0 = \lambda/15$. Dielectric permittivity of the surrounding medium was assumed to be $\epsilon_d = 1$. The schematic of the endoscope is shown in Fig. 1 (left). The EM wave is launched from a single-mode square $2\lambda/3 \times 2\lambda/3$ waveguide at $z = -10L_0$. We have chosen a circularly polarized incident wave to avoid polarization sensitivity of a square array of wires. The scattering metal sphere's center is at $z_{\text{obj}} = -0.7D$, $x = x_{\text{obj}}$, $y = y_{\text{obj}}$. Two lateral sphere positions have been simulated: (a) ($x_{\text{obj}} = -d/2$, $y_{\text{obj}} = 0$), and (b) ($x_{\text{obj}} = d/2$, $y_{\text{obj}} = d/2$). The respective intensity distributions of the $|\vec{E}_\perp|^2$ at the end of the endoscope ($z = 19L_0$) shown in Figs. 3(a) and 3(b) confirm the earlier made statement about the sampling nature of TEM-based imaging: only the mere presence of a scattering sphere inside a given elementary cell is detected, with the details of the scatterer's shape lost. From Fig. 3(b) it is clear that the imaging square pixel is defined by four nearest wires. The peak intensity in the imaging plane is higher by 1 order of magnitude when the scattering object is present compared with the case of a multiwire endoscope with no scattering object: $I_{\text{scatt}}/I_{\text{wire}} = 10$. The latter intensity is another 5 orders of magnitude higher than when the wires are removed from the waveguide: $I_{\text{wire}}/I_{\text{wg}} = 10^5$.

Next, we demonstrate that an endoscope based on the *tapered* metal wire array shown in Fig. 1 (right) is capable of magnification and demagnification. One obvious application of image magnification is a sensor collecting EM fields from highly subwavelength objects in the immediate proximity of the endoscope's tip and transforming them into a much larger detectable image. Image demagnification can be applied to surface patterning and lithography: a complex large mask can be placed close to the wide base of

the endoscope and projected or focused towards the tip creating a highly subwavelength intensity distribution in the tip's vicinity. We have simulated a pyramid-shaped metallized fiber threaded by a 3×3 array of metallic wires. The endoscope's base has a $10L_0 \times 10L_0$ square cross section (where, as before, $L_0 = \lambda/15$), wires' separation is $d = 3L_0$, wires' diameters are $w = 2L_0$. All these dimensions are proportionately scaled down by a factor 5 at the tip. The purpose of this simulation is to illustrate image magnification and demagnification by a factor 5. As in the nontapered case, the tapered endoscope is terminated on both ends by a single-mode $(2\lambda/3 \times 2\lambda/3)$ metallic waveguide. A practical multichannel endoscope will have a much larger (e.g., 25×25) number of metal wires.

For a magnification demonstration, a small metallic sphere with diameter $D_{\text{small}} = \lambda/25$ is placed at a distance $\Delta z = 0.7D_{\text{small}}$ above the endoscope's tip halfway between the central wire and the next one on the left. The sphere is illuminated from the top by a circularly polarized electromagnetic wave. The image of $|\vec{E}_\perp|^2$ taken at $z_{\text{im}} = L_0$ (slightly above the endoscope's base) is shown in Fig. 4(a). The sphere's image (or that of any strong scatterer) magnified by a factor 5 appears as an enhanced field in the image plane. The following intensity contrasts are found: $I_{\text{scatt}}/I_{\text{wires}} = 3$ and $I_{\text{wires}}/I_{\text{wg}} = 10^3$.

The opposite process (demagnification, or image focusing) can also be demonstrated using the same tapered endoscope. A metallic sphere with the diameter $D_{\text{large}} = \lambda/5$ is placed at a distance $\Delta z = 0.7D_{\text{large}}$ below the endoscope's base halfway between the central wire and the next one on the left. The image located in the plane of the tip [hot spot shown in Fig. 4(b)] is spatially compressed by a factor 5. Despite the fact that the electromagnetic wave propagates through a very narrow waveguide, field intensity in the hot spot is about the same as that of the incident wave. Had the coupling efficiency of the incident wave into TEM waves been close to unity, one would expect an intensity increase by a factor 25 due to the narrowing of the endoscope's area. That this is not happening is attributed to the low coupling efficiency because of the subwavelength size of the scattering sphere. Nevertheless, this simulation illustrates that extremely subwavelength intensity landscapes can be created near the tip of a tapered nanowire array. The following intensity contrasts are found: $I_{\text{scatt}}/I_{\text{wires}} = 15$ and $I_{\text{wires}}/I_{\text{wg}} = 10^5$. Cross talk between metal wires in a tapered endoscope can potentially result in image spreading. Numerical simulations (not shown) indeed demonstrate that for rapidly tapered endoscopes (Z/X aspect ratio of order one and smaller) the image is no longer confined. Image spreading is not a factor for gently tapered endoscopes considered above.

All simulations presented in this Letter were performed using the PEC assumption. This assumption is highly accurate in the far-infrared and THz frequency ranges. It is, however, instructive to check whether the concept of a multiwire endoscope could be potentially extended to mid-infrared wavelengths. Below we demonstrate that the TEM modes of an array of PEC wires has a low-loss dispersionless surface plasmon polariton (SPP) counterpart in the optical part of the spectrum. We consider $\lambda = 5$ μm because of the importance of this wavelength to chemical sensing [24] as well the availability of low-loss silica fibers. We have used a commercial finite elements code COMSOL to compute the propagation constants of such SPPs assuming a square array of gold wires ($d = 0.5$ μm, $w = 0.33$ μm, $\epsilon_{\text{Au}} = -916 + 228i$) embedded in a dielectric fiber with $\epsilon_d = 2.25$. An endoscope based on this wire array provides $\lambda/10$ spatial resolution. Simulation results are shown in Fig. 2 where the blue

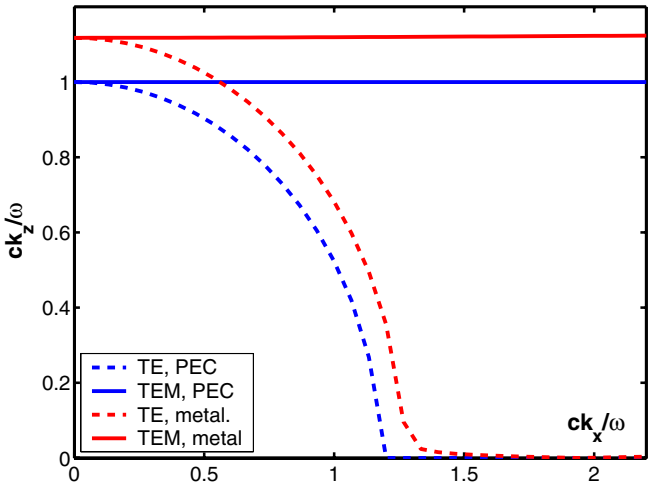

FIG. 2 (color online). Dispersion curves for two types of electromagnetic waves supported by an infinite square array of metallic wires (diameter $w = \lambda/15$, period $d = \lambda/10$, vacuum wavelength $\lambda \equiv 2\pi c/\omega$) imbedded in a dielectric with $\epsilon_d = 2.25$. Blue lines: wires are PECs. Red lines: gold wires with $\epsilon_{\text{Au}} = -916 + 228i$ corresponding to $\lambda = 5$ μm.

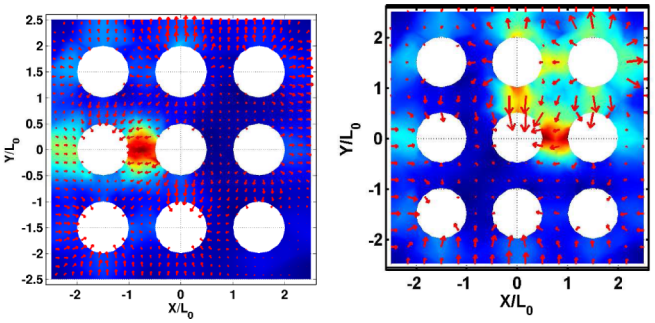

FIG. 3 (color online). Transport of the image of a metal sphere (diameter $D = \lambda/10$) by a straight subwavelength endoscope shown in Fig. 1(left) consisting of a 3×3 wire array placed inside a square subwavelength metallic waveguide of the width $W = \lambda/3$. The sphere's center is at $z_{\text{obj}} = -0.7D$, $x = x_{\text{obj}}$, $y = y_{\text{obj}}$. Shown are the color-coded $|\vec{E}_\perp|^2$ profiles in the imaging plane $z = 4\lambda/3$ for (a) $(x_{\text{obj}} = -d/2, \quad y_{\text{obj}} = 0)$, and (b) $(x_{\text{obj}} = d/2, y_{\text{obj}} = d/2)$. Arrows represent the electric field.

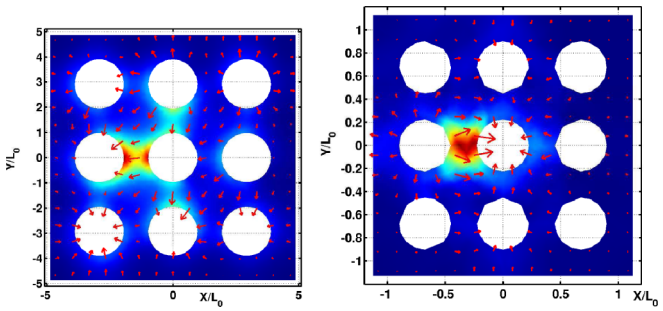

FIG. 4 (color online). Applications of a tapered endoscope from Fig. 1 (right): image magnification and demagnification by a factor 5. (a) Image magnification: image of a small metal sphere (diameter $D_{\text{small}} = \lambda/25$) placed just above the tip at ($x_{\text{obj}} = -D_{\text{small}}/2$, $y_{\text{obj}} = 0$) is transported to the base plane. (b) Image demagnification: image of a larger metal sphere (diameter $D_{\text{large}} = \lambda/5$) placed just below the base at ($x_{\text{obj}} = D_{\text{large}}/2$, $y_{\text{obj}} = 0$) is transported to the tip.

curves correspond to the idealized (PEC) wires while the red curves correspond to the realistic plasmonic wires. The similarity between these two sets of curves is obvious. Quantitatively, it is found that for the TEM-like SPPs $ck_z(\vec{k}_\perp = 0)/\sqrt{\epsilon_d}\omega = 1.12 + 0.01i \equiv \chi_r + i\chi_{\text{im}}$ confirming their low-loss nature. Very weak dependence of k_z on $\vec{k}_\perp$ (*transverse dispersion*) of the SPPs was confirmed by calculating $k_z(k_x = \pi/d)$ at the edge of the Brillouin zone: $G \equiv [k_z(k_x = \pi/d) - k_z(\vec{k}_\perp = 0)]/k_z(\vec{k}_\perp = 0) = 7 \times 10^{-3}$. Note that the computations are performed for a fixed frequency, and, therefore, the transverse dispersion is not related to the more common phenomenon of chromatic dispersion. Spatial dispersion is caused by the finite skin depth and, therefore, increases for shorter wavelengths and correspondingly thinner wires

The validity of the ideal TEM description is justified for transport distances of $L < \lambda/2\pi\epsilon_d \times \min(\pi/G, 1/\chi_{\text{im}})$. Ohmic losses over distances $L > \lambda/2\pi\epsilon_d/\chi_{\text{im}} \approx 8\lambda$ reduce the transmitted light intensity but do not necessarily deteriorate the spatial resolution ($\lambda/10$) of the image. Transverse dispersion, however, reduces spatial resolution below $\lambda/10$ for $L > 42\lambda$. For higher spatial resolutions, however, transverse dispersion become more severe than Ohmic losses: an endoscope must be shorter than $L = 5.5\lambda$ if the spatial resolution of $\lambda/25$ is desired. We conclude from these results that, although the classic dispersion relation $k_z = \sqrt{\epsilon_d}\omega/c$ for TEM waves is no longer strictly satisfied for plasmonic wires, the TEM-like SPPs are sufficiently low-loss and dispersionless that the performance of the untapered and tapered multiwire endoscopes described in this Letter are barely affected. The actual fabrication of tapered silica fibers threaded by metallic wires can proceed according to the recently developed [25] high pressure chemical vapor deposition technique.

In conclusion, we have demonstrated the possibility of a novel deeply subwavelength image manipulation (focusing and magnification) based on a tapered array of metallic wires. Such tapered endoscopes may find a variety of applications in the areas of infrared imaging, guiding, and focusing.

This work is supported by the ARO MURI No. W911NF-04-01-0203, the AFOSR MURI No. FA9550-06-1-0279, and the DARPA Contract No. HR0011-05-C-0068.

*gena@physics.utexas.edu

[1] K. Kneipp, Y. Wang, H. Kneip, L. T. Perelman, I. Itzkan, R. R. Dasari, and M. S. Feld, Phys. Rev. Lett. **78**, 1667 (1997).
[2] A. M. Michaels, J. Jiang, and L. Brus, J. Phys. Chem. B **104**, 11 965 (2000).
[3] T. Ichimura, N. Hayazawa, M. Hashimoto, Y. Inouye, and S. Kawata, Phys. Rev. Lett. **92**, 220801 (2004).
[4] J.-X. Cheng, L. D. Book, and X. S. Xie, Opt. Lett. **26**, 1341 (2001).
[5] P. Berini, Phys. Rev. B **63**, 125417 (2001).
[6] S. I. Bozhevolnyi, V. S. Volkov, E. Devaux, J.-Y. Laluet, and T. W. Ebbesen, Nature (London) **440**, 508 (2006).
[7] J. A. Dionne, H. J. Lezec, and H. A. Atwater, Nano Lett. **6**, 1928 (2006).
[8] D. B. Shao and S. C. Chen, Appl. Phys. Lett. **86**, 253107 (2005).
[9] J. B. Pendry, Phys. Rev. Lett. **85**, 3966 (2000).
[10] N. Fang, H. Lee, C. Sun, and X. Zhang, Science **308**, 534 (2005).
[11] D. O. S. Melville and R. J. Blaikie, Opt. Express **13**, 2127 (2005).
[12] T. Taubner, D. Korobkin, Y. Urzhumov, G. Shvets, and R. Hillenbrand, Science **313**, 1595 (2006).
[13] S. A. Maier, M. Brongersma, and H. Atwater, Appl. Phys. Lett. **78**, 16 (2001).
[14] M. I. Stockman, Phys. Rev. Lett. **93**, 137404 (2004).
[15] A. Ono, J. Kato, and S. Kawata, Phys. Rev. Lett. **95**, 267407 (2005).
[16] L. Carbonini, IEEE Trans. Microwave Theory Tech. **40**, 665 (1992).
[17] P. A. Belov and M. G. Silveirinha, Phys. Rev. E **73**, 056607 (2006).
[18] F. Keilmann, Infrared Phys. Technol. **36**, 217 (1995).
[19] K. Wang and D. M. Mittelman, Nature (London) **432**, 376 (2004).
[20] J. B. Pendry, A. J. Holden, W. J. Stewart, and I. Youngs, Phys. Rev. Lett. **76**, 4773 (1996).
[21] A. K. Sarychev, R. C. McPhedran, and V. M. Shalaev, Phys. Rev. B **62**, 8531 (2000).
[22] P. A. Belov, R. Marques, S. I. Maslovski, I. S. Nefedov, M. Silveirinha, C. R. Simovski, and S. A. Tretyakov, Phys. Rev. B **67**, 113103 (2003).
[23] M. A. Shapiro, G. Shvets, J. R. Sirigiri, and R. J. Temkin, Opt. Lett. **31**, 2051 (2006).
[24] M. Brehm, T. Taubner, R. Hillenbrand, and F. Keilmann, Nano Lett. **6**, 1307 (2006).
[25] P. J. A. Sazio *et al.*, Science **311**, 1583 (2006).